Thermochromic photoluminescent 3D printed polymeric devices based on copper-iodide clusters

Matteo Gastaldi, Ignazio Roppolo, Annalisa Chiappone, Claudio Garino, Andrea Fin, Matteo Manachino, Paolo Sirianni, Guido Viscardi, Luciano Scaltrito, Marco Zanetti, Silvia Bordiga, Claudia Barolo*

M. Gastaldi, Prof. C. Garino, Prof. G. Viscardi, Prof. M. Zanetti, Prof. S. Bordiga, Prof. C. Barolo.
Department of Chemistry and NIS Interdepartmental Centre and INSTM Reference Centre, Via Pietro Giuria 7, University of Turin, Turin 10125, Italy.

Dr. I. Roppolo, Dr. A. Chiappone, Prof. L. Scaltrito
Department of Applied Science and Technology, Politecnico di Torino, Corso Duca degli Abruzzi 24, 10129 Turin, Italy

Dr. I. Roppolo, Dr. A. Chiappone
Center for Sustainable Future Technologies, Istituto Italiano di Tecnologia, Via Livorno 60, 10144, Turin, Italy

Dr. A. Fin.
Department of Drug Science and Technology, Via Pietro Giuria 11, University of Turin, Turin 10125, Italy.

M. Manachino, P. Sirianni

E-mail: ignazio.roppolo@polito.it

Keywords: DLP 3D printing, luminescent copper clusters, polymeric waveguides, functional polyacrylate materials, additive manufacturing, smart materials

In this work, optically-active devices are fabricated by Digital Light Processing (DLP) 3D printing technology employing copper-iodide photoluminescent clusters as smart dyes in the photocurable formulation. These compounds are easy to synthesize, low cost and possess large stoke shift, thermochromic and rigidochromic properties, which make them particularly appealing for the development of optical devices. By dispersing such compounds in photocurable formulations, the same properties are transferred to polymeric materials, enabling the production of a large range of devices. Absorbing in the UV range and emitting in the visible range, those clusters show twofold advantages: on the one hand, competing with the photoinitiator for the light absorption, they allow a better control of the photopolymerization process, enabling the fabrication of precise structures; on the other hand these possesses

aesthetic properties, being transparent and then emitting light when irradiated. At last, functional structures, such as 3D printed polymeric waveguides (PWGs) and downshifting devices, are fabricated and investigated but even other uses can be envisaged, such as criogenic optical thermometers.

1. Introduction

Polymeric photoluminescent waveguides (PWGs) are nowadays used in a broad range of applications, such as in light-emitting devices (LEDs),[1] light-tunable photonics,[2,3] optics,[4] photonic integrated circuits,[5] communications,[6] biomedicals[7,8] and even sensors.[9–12] The possibility to exploit the thermal and mechanical stability of the polymeric matrices, joined to the flexibility of the final device and the inexpensiveness of the materials, has promoted the use of polymers as materials for innovative waveguides[10] but still a lot can be done, especially in the fabrication of complex devices.

In the last 30 years, many fabrication processes have been developed to shaping those materials, such as lithography,[5] controlled deposition[13] and electrospinning[14]. Generally PWGs are fabricated employing conjugated polymers, that emits thanks to the long-range π-electron conjugation.[15] This strategy is largely explored, however it presents some drawbacks, such as high costs, the necessity of usually complex chemical synthesis, the not-trivial relationships between structure and properties,[16,17] the limits of the manufacturing methods[18] and finally the presence of amorphous domains and defects.[19] An alternative method to produce PWGs consists in the dispersion of photoluminescent fillers, such as organic or inorganic molecules and complexes, in an optically-inert polymeric matrix. The use of this loading method may lead to several advantages like high optical transparency, reduced costs and easy processability.[15]

With the recent improvement of 3D printing technologies, the became easier the possibility to build really customized optical elements with complex three-dimensional shapes, maintaining high fidelity to the CAD virtual project. Additional functionalities can be also conferred through

the synthesis and development of functional and printable polymeric materials[20] with the introduction of dyes and fillers, as reported in some recent reviews.[21-23]

Typically three-dimensional printed (3DP) PWGs were produced using Fused Filament Fabrication (FFF)[24-26] or Direct Ink Writing (DIW)[27] techniques. In those cases, the emitting properties were obtained introducing transition metals,[28] rare earth[29,30] and organo-lanthanide complexes[31] or organic molecules[32] as guests. Only recently, the use of such compounds has found applications in light induced 3D printing (which comprehends Stereolithography (SLA) and in Digital Light Processing (DLP) printers) to obtain coloured emitting polymers[20] with complex and accurate shapes.[33] As an example, Frascella et al.[34] demonstrated the possibility to fabricate PWGs using DLP, copolymerizing organic emitter with an optically inert polymer. However, the residual coloured matrix and the reduced Stokes shift of the photoluminescent moieties represent a limit in the use of this 3DP material as PWGs.

The application of a printable polymeric matrix embedding emitters that are able to absorb in the UV range and emit in the visible range, showing high stability under light irradiation, high quantum yield and very low costs can represent a step forward in the realization of efficient PWGs. Thanks to DLP method and the possibility to easily customize the material's properties playing on the different components,[35] very complex and high-defined devices can be carried out.[20]

Furthermore, light sensitive compounds can play a twofold positive effects in materials for light-induced 3D printing: on the one hand, those can impart new functionalities, even at relatively low amounts, on the other, those can be used to improve the printing precision, controlling the light absorption and thus the photopolymerization process, avoiding uncontrolled curing.[23] Example of this twofold use can be found in many applications, such as laser-tunable elastic modulus,[35] photo-activated gas permeability,[36] light-emitting materials[20] and UV or temperature-responsive polymers.[37] Moreover, since light-based 3D

printers operates at room temperature, any temperature-induced dye degradation can be avoided. Unfortunately, dyes may reduce the transparency of the structures, conferring a colour to the polymeric matrix, which can be highly undesired, especially in optical applications.

In this work, we investigated the introduction of copper iodide clusters of general formula $[Cu_4I_4L_4]$ (L = phosphine-based ligands **Figure 1**) in an acrylic 3DP polymeric matrix, able to guide the irradiation from one end to the other, converting it from UV to visible light. Copper-halide based clusters are well-known and deeply studied compounds to produce luminescent materials,[38] thanks to their intriguing thermal-depending photophysical properties[39-42] according to the different ligands used.[43] These species are stimuli responsive since they can change their emission according to environmental, mechanical and temperature variations.[44,45] Furthermore, these compounds display very high quantum yields,[46] an absorption band in the UV range, a large Stokes shift, high stability, in particular for compounds containing iodine, and they also show mechanochromic and rigidochromic behaviours.[47] Moreover, the low toxicity of these compounds, compared to other transition metals, the facile synthesis with good yield and the peculiar optical properties of these compounds make them very promising in the use as thermometer[46] or in many other applications.[43,48] In this context, these compounds are suitable to generate almost transparent PWGs.

3D printable resins were carried out to investigate the photopolymerization kinetics and optical properties of the bisphenol A ethoxylate diacrylate (BEDA), used as printable monomer, containing different concentrations of copper-iodide clusters as smart dyes. Then, the 3D printing process was performed, finding the optimal parameters to fabricate precise complex devices that were fully characterized, taking in particular account optical and emissive properties. The high resolution achieved for the final device and the ability to guide the irradiation through the polymeric medium with a good efficiency will be also demonstrated, as well as the relative effect of temperature on the guiding efficiency. To the best of our

knowledge, this is the first time that copper-based clusters are introduced in 3D printable formulations.

2. Experimental

2.1. Materials

Bisphenol A ethoxylate diacrylate (BEDA) (M_n = 512, EO/phenol = 2), 2-hydroxy-2-methylpropiophenone (HMPP), toluene, chloroform, dichloromethane (DCM) and acetonitrile (ACN) were purchased from Sigma-Aldrich and used as received. The two copper iodide clusters $[Cu_4I_4(PPh_3)_4]$ **1** and $[Cu_4I_4(PPh_2(CH_2)_2CH_3)_4]$ **2** depicted in **Figure 1** were synthetized according to the procedures and matched the reported characterizations.[44, 49]

2.2. Formulations

Six formulations containing different concentration (0.1, 1.0 and 5.0 % w w^{-1}) of each copper-based cluster were prepared as follows. Each cluster were introduced as solid in a vial (10 mL) containing BEDA (5.0 g) liquid monomer. DCM (1.0 mL) was introduced into the formulation and all the vials were stirred for 1 hour at 50 °C and then sonicated in an ultrasonic bath for 1 hour more, until homogeneous solutions were obtained. The same procedure was followed to prepare a blank formulation without the introduction of copper cluster, used as reference. Before printing, the photoinitiator was added (1.0 % w w^{-1}) and the solution was sonicated for 5 minutes more.

2.2. 3D printing process

The printing process was carried out with Asiga DLP-3D printer (Max-UV) with nominal X–Y pixel resolution of 27 μm and the minimum Z-axis control of 1 μm. Light intensity of 25 mW cm^{-2} and layers slicing of 25 μm were the optimal parameters for the 3D printing process. The first 3 layers were irradiated for 15 seconds, to ensure the adhesion on the building platform. The irradiation exposure time was reduced to 10 seconds for all other layers. The printing process was performed a 25 °C and a post-curing process (5 minutes each side) was carried out

in a UV oven by Robofactory (light intensity 10 mW cm^{-2}) to obtain the almost total conversion of acrylic double bonds.

2.3. Characterization

^{1}H, ^{13}C and ^{31}P NMR spectra were recorded on a JEOL ECZR600 FT-NMR spectrometer (1H operating frequency 600 MHz) at 313 K and 298 K for **1** and **2**, respectively. ^{1}H and ^{13}C chemical shifts are reported relative to TMS ($\delta = 0$) and referenced against solvent residual peaks. Toluene-d_8 deuterated was used as deuterated solvent for **1**, while for **2** chloroform-d was employed.

UV-Visible absorption spectra were recorded on polymeric films in the 250 – 750 nm range with a Varian Cary 300 spectrophotometer. Photoemission spectra, luminescence lifetimes and quantum yields were acquired with a HORIBA Jobin Yvon IBH Fluorolog-TCSPC spectrofluorometer, equipped with a Quanta-φ integrating sphere. Solid state measurements were performed on 3D printed polymeric strips.

Photorheological tests were performed in real time during irradiation using an Anton Paar rheometer (Physica MCR 302) equipped with a Hamamatsu LC8 lamp (light emission in the UVA range, intensity 25 mW cm^{-2}). The measurements were performed in a plate-plate geometry equipped with quartz bottom plate. The gap between the plates was 200 μm. Oscillatory measurements were performed at 25 °C, at constant frequency (1 Hz) and amplitude (1 %). Amplitude sweep test (from 0.01 to 100 %, frequency 1 Hz) was preliminarily performed to evaluate the linear viscoelastic range.

ATR-FTIR spectra were collected with a Nicolet iS50 Spectrometer equipped with an attenuated total reflection (ATR). The range 4000-500 cm^{-1} was scanned (32 scans per spectra, resolution 2 cm^{-1}). The acrylic double bond conversion after the different stages was determined by the reduction of the peak centred at 980 cm^{-1} normalized by the aromatic signal at 1550 cm^{-1}.

Differential scanning calorimetry (DSC) measurements were performed with a Q200 (TA Instrument). The experiments were carried out between -20 to 80 °C with a heating rate of 20 °C min^{-1} and 10 °C min^{-1} as cooling rate. Thermal gravimetric analyses (TGA) were carried out with a Q600 (TA Instrument) on the polymeric film heating from 30 °C to 650 °C with a heating rate of 10 °C min^{-1} in air.

Insoluble fraction was measured by evaluating the weight loss of 3DP components after 24 h of chloroform extraction.

The precision of 3D printing process in complex structures structure was evaluated using a E4 3D scanner (3Shape) with scanning accuracy of 4 microns.

The efficiency of the light propagation into the PWGs were evaluated using, as optical power source, a LED LZ4-04UV0R OSRAM. The current source and electrical powermeter is a KEITHLEY 2602A SourceMeter, while the spectrometer is a USB4000 and the optical fiber is a FT600EMT - 0.39 NA, Ø600 µm Core Multimode Optical Fiber.

3. Result and discussion

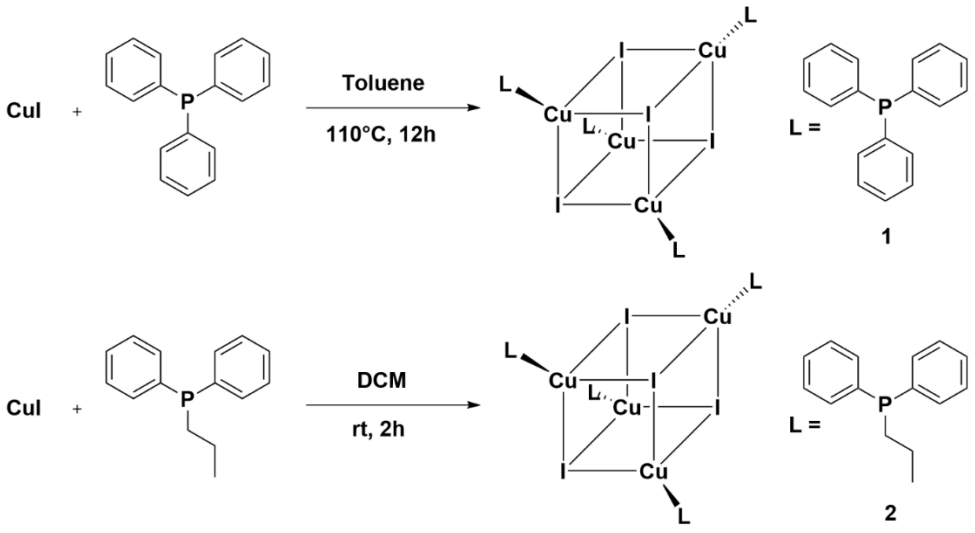

Figure 1. Synthesis of copper-based clusters

Two different copper-based clusters were synthetized to evaluate their dispersion into liquid formulations composed of BEDA as monomer and HMPP as photoinitiator. Both of the synthetized compounds have been considered in previously reported papers[39, 43-45, 47, 49-50] and

their synthetic schemes are reported in **Figure 1**. Despite the higher temperature and times needed to produce **1**, it presents higher quantum yield than **2** and it can be excited with a more UV-shifted wavelength.[49]

Different formulations were set up to evaluate the optimal concentration of copper clusters into the polymeric BEDA matrix. To increase the solubility and reduce viscosity, DCM was added to the formulation and it can be easily removed by evaporation during the printing process. Copper cluster **1** presented some solubility issues, due to its low solubility in almost every organic solvent at ambient temperature. A good dispersion can be achieved only for 0.1 % w w^{-1}, while for the formulation containing higher concentration, a large amount of cluster remained undissolved, making the resins cloudy (**Figure 2a**). UV light at 365 nm emphasized these solubility problems as depicted in **Figure 2b** in which a yellow emission can be detected only for 1.0 % and 5.0 % of **1**. For compound **2**, all solutions do not show any emitting property, demonstrating the excellent solubility into the liquid resin. In fact, as previously reported, both **1** and **2** are able to emit only in crystalline solid state, while they almost lose this property in solution,[49] as demonstrated by the emission spectra of liquid formulation containing 1.0 % w w^{-1} of both **1** and **2** (**Figure S1**). In this graph the insolubility of **1** is clearly visible by the emission spectrum while **2** is totally soluble and no emitting properties can be detected.

Based on these initial results, some photopolymerization tests were carried out irradiating the resulting formulations, except for 5.0 % of **1**, with UV light under inert atmosphere, to evaluate the homogeneity of the resulting films. All films (**Figure S2**) appeared transparent under ambient illumination and only the formulations containing up to 1.0 % of **1** produced a precipitation of the copper cluster into the polymeric solid matrix, as demonstrated by **Figure 2c-d** compared to the film with the same concentration of **2** under 365 nm lamp.

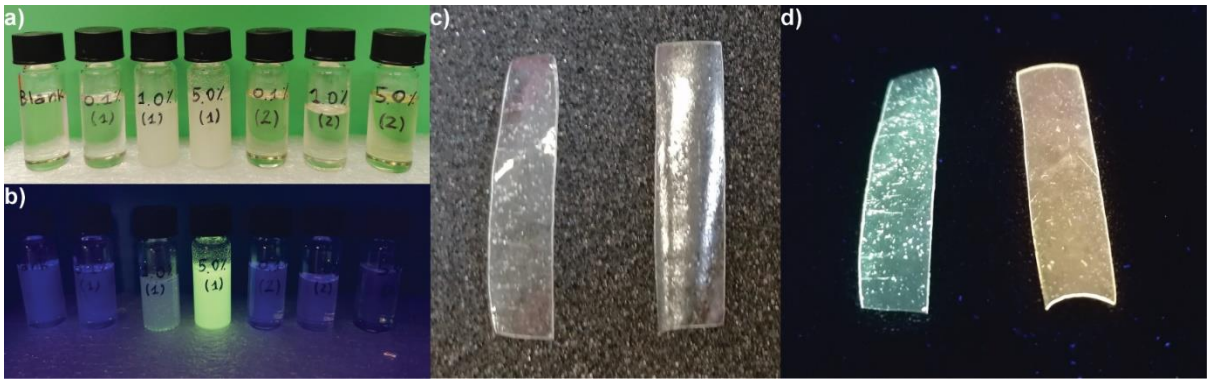

Figure 2. Formulations of monomer, photoinitiator, DCM and different concentrations of **1** and **2** under (a) ambient illumination and (b) under 365 nm UV lamp. The presence of insolubilized copper cluster is detected by the yellow emission of compound powder. c) Polymeric films with 1.0 % of both copper clusters **1** (left) and **2** (right). d) Emission of polymeric films with 1.0 % of **1** (left) and **2** (right) under 365 nm light.

As depicted in **Figure S3**, **1** presents higher emission at 330 nm excitation wavelength, but unfortunately very low solubility, which led to instable formulations during the printing. For these reasons, the following 3D printing process and all experiments were conducted only applying compound **2**.

Our previous results using conventional UV curing demonstrated that the introduction of less than 5.0 % w w^{-1} of copper clusters did not affect consistently the acrylic double bond conversion and the transparency.[38] Based on this report, different formulations were investigated by photorheology tests to evaluate the polymerization kinetics and transparency of the resulting 3DP films. As depicted in **Figure 3a**, the introduction of 1.0 % of **2** lead to almost transparent polymeric films that start to absorb irradiation under 400 nm. In the same figure, the absorption spectrum of the HMPP photoinitiator is reported, showing an absorption profile that overlap the copper-iodide cluster one. This overlapping can be useful in our process to control the printing precision and to avoid layers overcuring.[23] The transparency was also preserved after the post-curing process (**Figure S4**).

The concentration's effect of **2** on the photopolymerization kinetics can be evaluated by photorheology tests. As depicted in **Figure 3b**, the presence of the copper cluster **2** seems to do

no affect the photopolymerization up to a concentration of 5.0 % at the printer's LED power (25 mW cm^{-2}). This liquid mixture showed a higher storage modulus (*G'*), meaning a higher viscosity conferred by the cluster and a delayed start of the photopolymerization reaction with respect to other formulations.

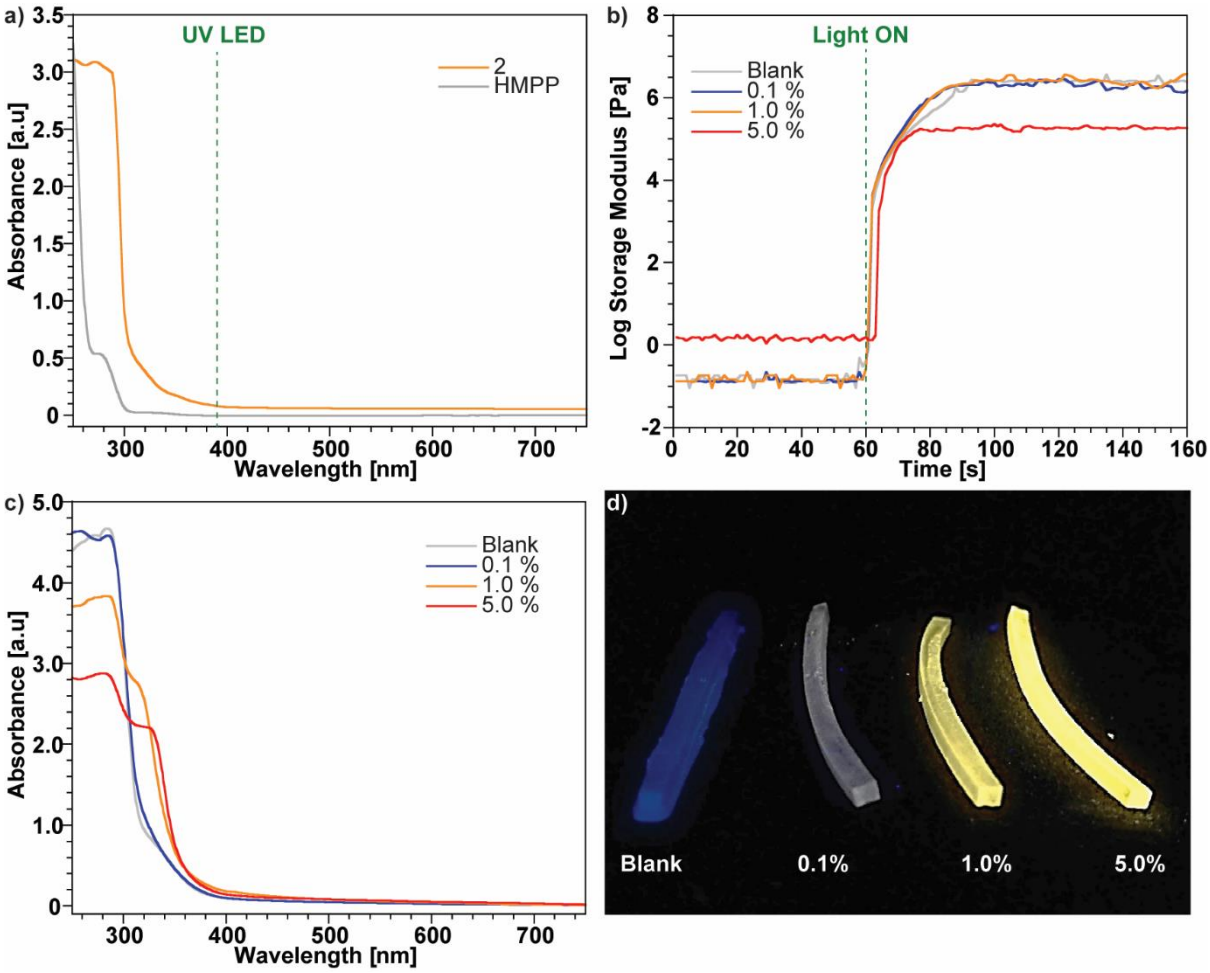

Figure 3. a) UV-Visible spectra of 3DP polymeric film containing 1.0 % of **2** overlapped to UV spectrum of photoinitiator in ACN. The UV emission of DLP 3D printer (385 nm) is represented by the straight dashed green line. b) Photorheological curves of liquid formulations containing increasing concentrations of **2**. The formulation without copper cluster represented the reference (Blank). c) UV-Visible spectra of 3D printed films containing different concentrations of **2**. d) Picture of 3DP polymeric strips with an increasing concentration of **2** under UV (365 nm) light.

Moreover, a reduced value of *G'* is reached after irradiation, that may be consistent with a reduced photopolymerization efficiency and a lower conversion of acrylic double bonds. These phenomena can be ascribed to the concurrent absorption of UV light between the photoinitiator and the emitter, which decrease the rate of photoinitiation and thus the final conversion.

To evaluate the real effect of **2** on the photopolymerization kinetics, photorheology tests were repeated at lower light intensity (0.5 mW cm^{-2}). In these conditions, the delayed start of photopolymerization for each formulation (**Figure S5**) was observed, indicating a clear effect of the copper clusters. On the other hand, all the considered formulations of copper cluster, including the one with 5.0 %, showed good transparency in the visible range, and this property was preserved in the 3DP matrices (**Figure 3c**).

3DP PWGs with an increasing content of **2** were produced, evalutating the good final resolution and their visible emitting properties under UV irradiation (**Figure 3d**). The blank and the sample containing 0.1 % of **2** show a blue emission due to the polymeric matrix (**Figure S6**) while with the addition of 1.0 % of **2** the emission start tuning to light yellow, reaching the maximum at 5.0 %. With 1.0 % good emitting properties can be reached avoiding the efficiency reduction on the photopolymerization kinetics and preserving at the same time the mechanical and thermal properties of the polymeric matrix. The fabrication of these samples and the evaluation of the double bond's conversion allow the optimization of the 3D printing parameters, reported in **Table 1**.

To evaluate the efficiency of 3DP process, the acrylic double bonds conversion was evaluated by means of ATR-FTIR spectroscopy (the overlapped spectra are reported in **Figure S7**). As reported in **Table 1**, the presence of copper clusters did not affect the conversion after 3D printing process. These results were in good agreement with the conversion trend obtained for UV-cured coatings.[38] Despite the lower values, it should be noted that the higher conversions in literature were obtained for longer irradiations and in nitrogen atmosphere, while 3D printing involves very short irradiation times and may suffer of oxygen inhibition, especially in external surfaces. Nevertheless, the measured values were compatible with an efficient 3D printing process and the obtained samples had a very low amount of uncured monomers, as demonstrated by gel content measurements (**Table 1**).

Table 1. Double bond conversions of 3DP films are reported before and after the post curing process in UV oven for 5 seconds each side. T_g and thermal degradation properties of the final post cured BEDA (blank) and polymers containing different concentrations of **2** (T_5 correspond to the temperatures at which the samples lose 5.0 % of weight) are described.

Compound 2 content [%]	-C=C- Conversion post cured film[a)] [%]	Insoluble fraction [%]	T_g [°C]	T_5 [°C]
Blank	80	99	35.4	313
0.1	79	99	48.4	274
1.0	78	99	43.5	288
5.0	70	95	47.1	247

The thermal properties of the 3D printed materials were also investigated by DSC and TGA tests. Those demonstrated that the introduction of the clusters induced an increase of the glass transition temperature (T_g), probably related to increased hindering of chains movements by the clusters and slight reduction of thermal stability. As reported in **Table 1** the T_g raised nearly 10 °C by just adding 0.1 % of **2.** This means that the introduction of copper iodide clusters affected the stiffness of the polymeric network (**Figure S8**). TGA analyses demonstrated that copper clusters do not affect the thermal stability of the final 3DP devices (**Figure S9**).

The photoluminescence of the 3DP polymeric matrix containing 1.0 % of **2** has been evaluated. As expected, the material exhibits a large Stokes Shift (**Figure 4a**) and a thermochromic luminescence, characterized by two temperature-dependent emissions (**Figure 4b**) typical of $[Cu_4I_4L_4]$ copper iodide clusters.[38,39] Under UV excitation (330 nm) at room temperature, the printed composite displays a single bright yellow luminescence. This low-energy band (LE) is attributed to a ‘‘cluster-centered’’ triplet excited state (3CC) and is independent of the nature of the ligand. Lowering the temperature to 77 K, a structured deep-blue emission appears at higher energy (high-energy band, HE), alongside the LE band. The HE band is assigned to an iodide-to-phosphine ligand charge-transfer transition (XLCT).[51] The yellow emission is completely recovered when the sample is warmed up, indicating a perfectly reversible thermochromism. Varying the temperature, the emission curves evidence an isosbestic point at 520 nm, indicating a thermal equilibrium between the LE and HE excited states. This implies a

very high coupling of the two emission states leading to a perfectly controlled thermochromic luminescence, in a large temperature range.

The quantum yields (QY) were calculated on polymeric films containing 1.0 % of each copper complexes. For both samples a 30 % of QY was reached (excitation wavelength 330 nm): this value is lower than the one reported in literature for the crystalline solid state, and it could be addressed to the concurrent absorption of the polymeric matrix at the same wavelength, as demonstrated in **Figure 3c** (grey line) and in **Figure S6**.

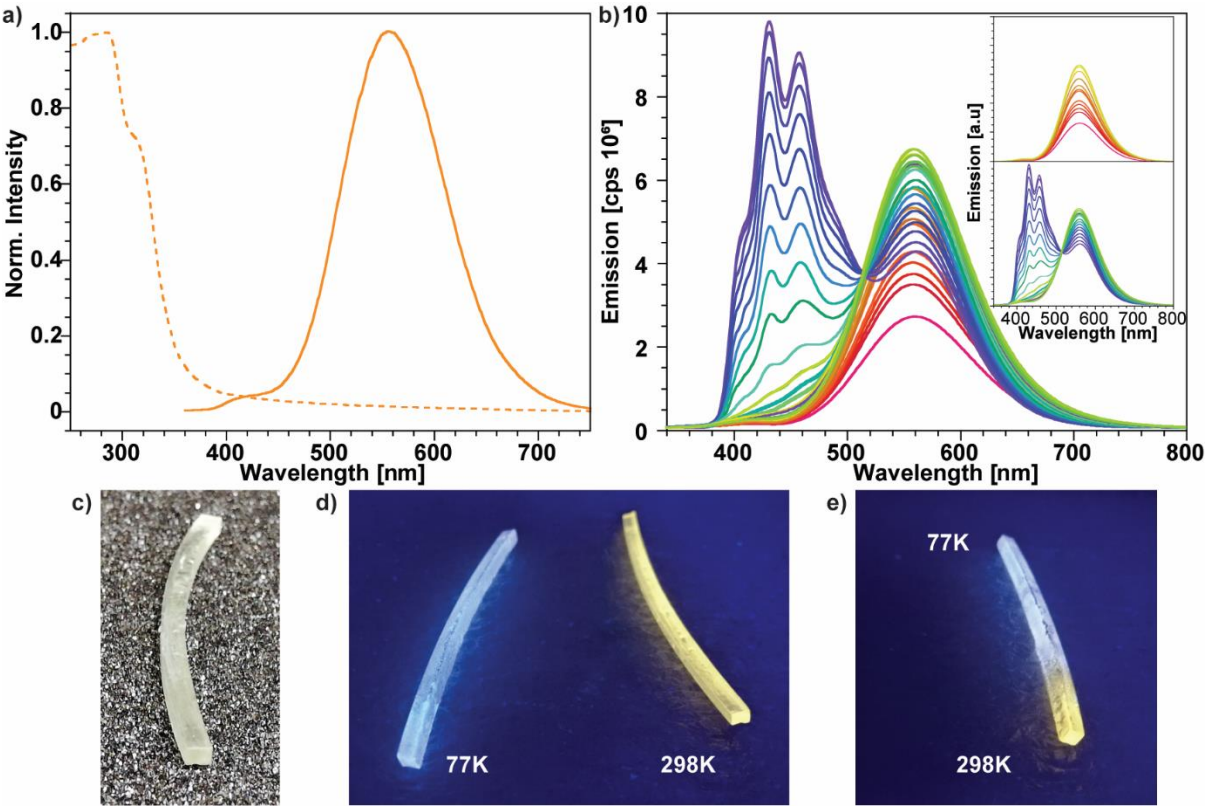

Figure 4. a) Absorption (dashed) and emission (solid) spectra of 3DP film containing 1.0 % of **2**. b) Temperature-dependent luminescence spectra of **2** (λ_{ex} = 330 nm, temperature from room temperature to 77 K). The two insets reported the separated first (top) and second (bottom) emission wavelengths. 3DP polymeric waveguide under ambient light (c), under UV (365 nm) light at different temperatures (77 K and 298K) and partially immersed in liquid nitrogen (e).

The lifetime of the HE and LE excited states have been also evaluated by time-correlated single photon counting. The measured lifetimes for the two emissions were τLERT/77K = 9 μs, τ1HE77K = 0.6 ms, τ2HE77K = 3.3 ms, in accordance with the phosphorescent nature of the two triplet excited states. The results obtained on the 3DP polymeric matrix confirmed those

previously reported for the fluorophore **2** incorporated in acrylic materials.[38] This was a clear indication that the integrity of the embedded clusters was preserved during the whole DLP process.

Temperature-dependent emission was also clearly detectable as demonstrated below. The 3DP component (**Figure 4c**) containing 1.0 % of **2** was irradiated and completely (**Figure 4d**) or partially (**Figure 4e**) immersed in liquid nitrogen. It is possible to observe with naked eyes the difference in the emission, which suggest also a possible exploitation of this 3DP structures as optical sensor for cryogenic temperatures.

Then, to evaluate the resolution of the final devices, more complex shapes were 3DP using the same optimized parameter, reported in **Table 1**, demonstrating the possibility to print very complex structures (**Figure 5a**) that keep the peculiar photoluminescent properties of the cluster (**Figure 5b**). The light diffuser structure was also investigated by 3D scanner, to evaluate the CAD fidelity. In **Figure 5c** a comparison between the CAD virtual project (**Figure S10**) and the 3D image of the real 3DP device is depicted, showing the great resolution and fidelity to the project with a displacement at about ± 0.050 mm in the green zones and ± 0.100 mm in the yellow and light blue one. The most evident defects were in the bottom part that represent the first layers built during the printing process (**Figure S11**). Those layers are over exposed to ensure the adhesion of the growing object to the printing platform, inducing polymerization even outside the irradiated areas, leading to loss of precision. Regarding the inner parts, those are blind points for the 3D scanner, so that volume cannot be considered meaningful for fidelity evaluation. The displacement data are reported on the top part of **Figure 5c**.

We have demonstrated the versatility and the good final resolution of the 3DP devices containing copper clusters, fabricating a complex-shaped object: under UV irradiation this device was able to diffuse yellow visible light and it can be used as a downshifter of UV LEDs, able to change at the same time its photoluminescent properties according to the temperature.

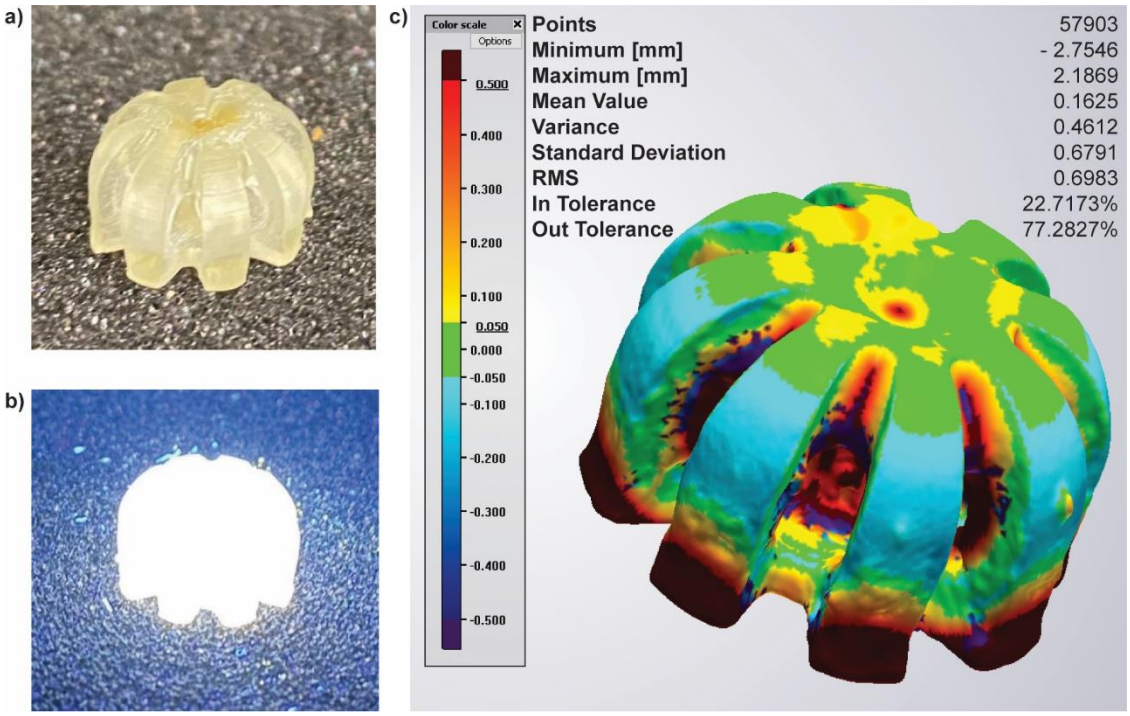

Figure 5. 3DP device with 1.0 % of **2** (a) under ambient and (b) 365 nm UV light. c) The 3D image obtained with 3D scanner with the evaluation of the displacement between the CAD project and the real device.

3DP PWGs with different lengths containing 1.0 % of **2** were fabricated to evaluate the conversion of UV irradiation given by a 365 nm LED into visible light and the guiding efficiency through the polymeric matrix. The lengths used were 2, 3 and 5 cm, which is the maximum that can be carried out due to the configuration of the 3D printer used.

Two different configurations, called direct and side pumping, were investigated changing the position of the UV source to evaluate the guiding properties. Sketch representations of these experimental setups are reported in **Figure S12**. The measurement conditions of each sample, the voltage used and the relative incident power density are reported in **Table 2**.

Table 2. Measurement conditions of LED spectrum and for each configuration used to evaluate the emitting properties of the PWGs at different lengths.

Measurement type	Measure	Excitation Current [mA]	Led Voltage Drop [V]	Incident power density [mW/mm^2]
LED	Led Spectrum	8	3.09	
DIRECT PUMPING	Sample 2 cm	300	4.35	94.97
	Sample 3 cm	300	4.01	94.97

	Sample 5 cm	**300**	**4.15**	**94.97**
SIDE PUMPING	**Sample 2 cm**	**800**	**5.29**	**223.74**
	Sample 3 cm	**800**	**5.29**	**223.74**
	Sample 5 cm	**800**	**5.28**	**223.74**

The emitting properties were also studied to evaluate the effective absorption of the UV LED irradiation by the copper cluster, the guiding through the polymeric matrix and the emission of visible irradiation at the end of the PWG for both configurations. The spectra direct and side pumping are depicted in **Figure 6a-b** while the emission of UV LED centered at 365 nm is reported in **Figure S13**. The ratio between LED and visible peaks areas were depicted in inset of **Figure 6a** in which a reduction of LED intensity and the relative increase of the visible irradiation is clearly visible. In fact, for the direct pumping configuration, the LED peak decrease with the length of the PWG due to the progressive absorption of the irradiation by the copper clusters and, in consequence, the visible irradiation intensity increased. Vice versa, for side pumping geometry the LED irradiation was not visible since the shorter length. Nevertheless, the direct pumping as well as the presence of the LED emission, presented a reduction of the visible irradiation according to the increase of the PWG's length, while the side pumping showed a reduced lateral dispersion of the irradiation (the blank emission spectra of 3DP PWG for both configurations are depicted in **Figure S14** are the experimental conditions are described in **Table S15**).

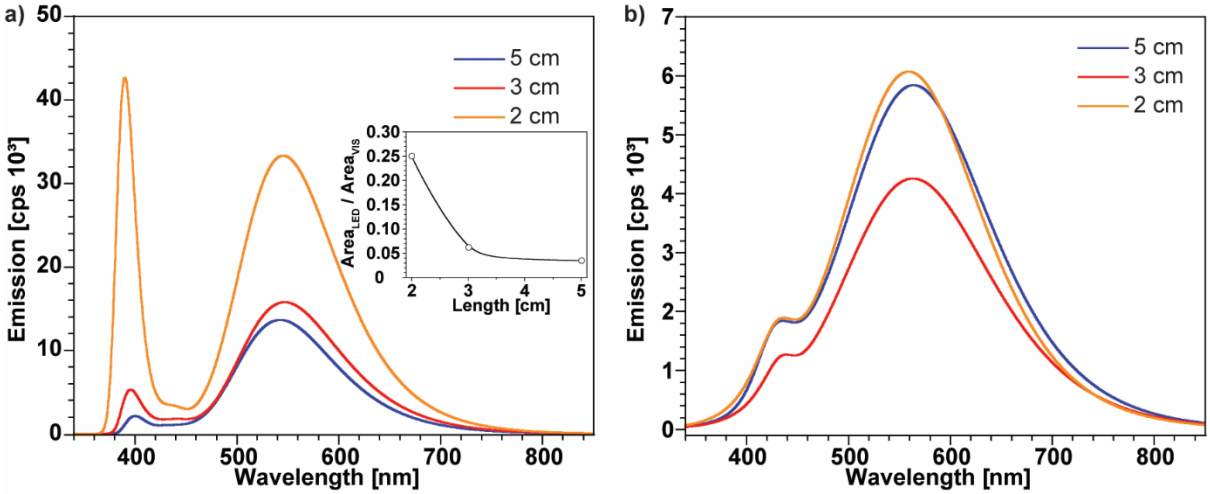

Figure 6. Emission spectra of (a) direct and (b) side pumping configurations of PWGs with different lengths. In the inset of (a) the ratios between the LED and visible emission areas are reported showing a clear disappearance of the LED's contribution and an increase of visible one.

Moreover, an evaluation of the effect of temperature using the direct configuration setup was also reported in **Figure 7**, using a Peltier cell to cool the PWG from 40°C to almost 13°C (the experimental setup is reported in **Figure S16** and the experimental conditions are reported in **Table S17**). In the graph the correlation between the area of each peak and the temperature is reported, showing an increase of the emission, as expected when the temperature decreased, even remaining in the almost common everyday temperature range.

From the previously reported graphs, the guiding of the irradiation was demonstrated, giving promising initial results that can path the way to improvements and other investigations in this field.

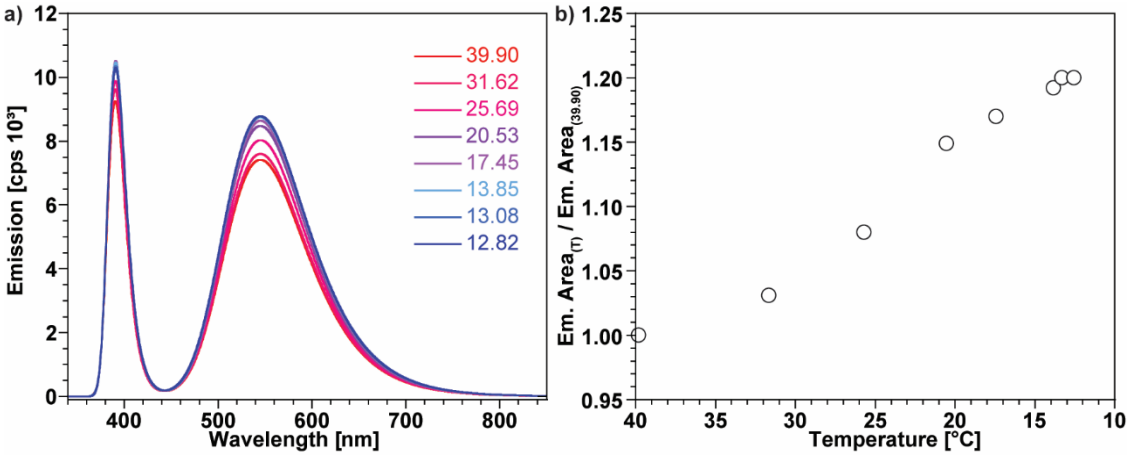

Figure 7. a) Emission spectra at different temperatures for 2 cm length PWG. b) The normalized emission areas at each temperature over the 39.90°C area to demonstrate a reduction in the emitting properties of the PWGs under increasing of temperature.

Conclusion

In this study, the application of copper-based clusters in 3D printable formulations to produce 3D printable photoluminescent devices is reported. The use of this compounds is of particular interest since it allows to avoid the use of more-known rare earth or transition metals complexes, which show synthetic issues, toxicity and higher costs than copper clusters. The embedding of such cluster in 3D printable polymers was demonstrating to be effective, producing materials that show both the dye's emitting properties and the transparency of polymeric matrix. Furthermore, thanks to the positive effect of the dye, high resolutions and complex shapes can be achieved in DLP 3D printer, obtaining devices that can be suitable as UV downshifter and as light diffusor. The efficiency of light guiding both for direct and side pumping UV irradiation is investigated, demonstrating initial promising results toward the use of these compounds in PWGs applications: optimal lengths of the device and improvements in the polymeric matrices are needed to achieve more optical transparency and higher guiding efficiency. Temperature-dependency of the emitting properties can lead toward applications even at very low temperature with a change in the emitting wavelengths.

References

[1] C. J. Yoo, J. Y. Park, J.-L. Lee, *ECS J. Solid State Sci. Technol.* **2018**, *7*, R190.

[2] S. Nocentini, D. Martella, C. Parmeggiani, D. S. Wiersma, *Adv. Optical Mater.* **2019**, *7*, 1900156.

[3] H. Xia, J. Cheng, L. Zhu, K. Xie, Q. Zhang, D. Zhang, G. Zou, *ACS Appl. Mater. Interfaces* **2019**, *11*, 15969–15976.

[4] C.-L. Sun, Z. Gao, K.-X. Teng, L.-Y. Niu, Y.-Z. Chen, Y. S. Zhao, Q.-Z. Yang, *ACS Appl. Mater. Interfaces* **2018**, *10*, 26526–26532.

[5] H. Ma, A. K.-Y. Jen, L. R. Dalton, *Adv. Mater.* **2002**, *14*, 1339–1365.

[6] J. W. Choi, Y. M. Ha, S. H. Lee, K. H. Choi, *J. Mech. Sci. Technol.* **2006**, *20*, 2094–2104.

[7] J. Feng, Q. Jiang, P. Rogin, P. W. de Oliveira, A. del Campo, *ACS Appl. Mater. Interfaces* **2020**, *12*, 20287–20294.

[8] J. Guo, C. Yang, Q. Dai, L. Kong, *Sensors* **2019**, *19*, 3771.

[9] J. Alamán, M. López-Valdeolivas, R. Alicante, C. Sánchez-Somolinos, *Sensors* **2019**, *19*, 2856.

[10] K. Jakubowski, W. Kerkemeyer, E. Perret, M. Heuberger, R. Hufenus, *Mater. Des.* **2020**, *196*, 109131.

[11] D. Niu, L. Wang, Q. Xu, M. Jiang, X. Wang, X. Sun, F. Wang, D. Zhang, *Appl. Opt.* **2019**, *58*, 1276–1280.

[12] S.-H. Oh, K.-D. Ahn, H.-Y. Choi, *Opt. Eng.* **2019**, *58*, 097104.

[13] T. Y. Hin, C. Liu, P. P. Conway, In 2007 Proceedings 57th Electronic Components and Technology Conference **2007**, 1737–1741.

[14] V. Fasano, M. Moffa, A. Camposeo, L. Persano, D. Pisignano, *Macromolecules* **2015**, *48*, 7803–7809.

[15] H. Xia, T. Chen, C. Hu, K. Xie, *Polymers* **2018**, *10*, 1086.

[16] C. A. Briehn, M.-S. Schiedel, E. M. Bonsen, W. Schuhmann, P. Bäuerle, *Angew. Chem. Int. Ed.* **2001**, *40*, 4680–4683.

[17] C. Gu, N. Huang, Y. Chen, L. Qin, H. Xu, S. Zhang, F. Li, Y. Ma, D. Jiang, *Angew. Chem. Int. Ed.* **2015**, *54*, 13594–13598.

[18] A. Garreau, J.-L. Duvail, *Adv. Opt. Mater.* **2014**, *2*, 1122–1140.

[19] S. Hayashi, *Polym. J.* **2019**, *51*, 813–823.

[20] F. Wang, Y. Chong, F. Wang, C. He, *J. Appl. Polym. Sci.* **2017**, *134*, 44988.

[21] M. Nadgorny, A. Ameli, *ACS Appl. Mater. Interfaces* **2018**, *10*, 17489–17507.

[22] J. A. Lewis, *Adv. Funct. Mater.* **2006**, *16*, 2193–2204.

[23] M. Gastaldi, F. Cardano, M. Zanetti, G. Viscardi, C. Barolo, S. Bordiga, S. Magdassi, A. Fin, I. Roppolo, *ACS Mater. Lett.* **2021**, *3*, 1−17.

[24] R. Stach, J. Haas, E. Tütüncü, S. Daboss, C. Kranz, B. Mizaikoff, *ACS Sens.* **2017**, *2*, 1700–1705.

[25] S. Khan, N. Vahabisani, M. Daneshmand, *IEEE Trans. Compon. Packag. Manuf. Technol.* **2017**, *7*, 70-80.

[26] F. Zhao, D. Cambié, J. Janse, E. W. Wieland, K. P. L. Kuijpers, V. Hessel, M. G. Debije, T. Noël, *ACS Sustain. Chem. Eng.* **2018**, *6*, 422-429.

[27] Q. Mu, C. K. Dunn, L. Wang, M. L. Dunn, H. J. Qi, T. Wang, *Smart Mater. Struct.* **2017**, *26*, 045008.

[28] N. Huby, J. Bigeon, Q. Lagneaux, M. Amela-Cortes, A. Garreau, Y. Molard, J. Fade, A. Desert, E. Faulques, B. Bêche, J.-L. Duvail, S. Cordier, *Opt. Mater.* **2016**, *52*, 196–202.

[29] Y. Xia, B. Xue, M. Qin, Y. Cao, Y. Li, W. Wang, *Sci. Rep.* **2017**, *7*, 1–10.

[30] Y. Ren, J. Feng, *ACS Appl. Mater. Interfaces* **2020**, *12*, 6797–6805.

[31] S. Moynihan, R. Van Deun, K. Binnemans, G. Redmond, *Opt. Mater.* **2007**, *29*, 1821–1830.

[32] Z. Li, P. Liu, X. Ji, J. Gong, Y. Hu, W. Wu, X. Wang, H.-Q. Peng, R. T. K. Kwok, J. W. Y. Lam, J. Lu, B. Z. Tang, *Adv. Mater.* **2020**, *32*, 1906493.

[33] D. Ahn, L. M. Stevens, K. Zhou, Z. A. Page, *ACS Cent. Sci.* **2020**, *6*, 1555–1563.

[34] F. Frascella, G. González, P. Bosch, A. Angelini, A. Chiappone, M. Sangermano, C. F. Pirri, I. Roppolo, *ACS Appl. Mater. Interfaces* **2018**, *10*, 39319–39326.

[35] I. Roppolo, A. Chiappone, A. Angelini, S. Stassi, F. Frascella, C. F. Pirri, C. Ricciardi, E. Descrovi, *Mater. Horiz.* **2017**, *4*, 396–401.

[36] M. Gillono, I. Roppolo, F. Frascella, L. Scaltrito, C. F. Pirri, A. Chiappone, *Appl. Mater. Today* **2020**, *18*, 100470.

[37] H. Xie, K.-K. Yang, Y.-Z. Wang, *Materials Today: Proceedings* **2019**, *16*, 1524–1530.

[38] I. Roppolo, E. Celasco, A. Fargues, A. Garcia, A. Revaux, G. Dantelle, F. Maroun, T. Gacoin, J.-P. Boilot, M. Sangermano, S. Perruchas, *J. Mater. Chem.* **2011**, *21*, 19106.

[39] S. Perruchas, X. F. Le Goff, S. Maron, I. Maurin, F. Guillen, A. Garcia, T. Gacoin, J.-P. Boilot, *J. Am. Chem. Soc.* **2010**, *132*, 10967–10969.

[40] B. Li, H.-T. Fan, S.-Q. Zang, H.-Y. Li, L.-Y. Wang, *Coord. Chem. Rev.* **2018**, *377*, 307–329.

[41] B. Xin, J. Sang, Y. Gao, G. Li, Z. Shi, S. Feng, *RSC Adv.* **2018**, *8*, 1973–1978.

[42] E. Cariati, E. Lucenti, C. Botta, U. Giovanella, D. Marinotto, S. Righetto, *Coord. Chem. Rev.* **2016**, *306*, 566–614.

[43] B. Huitorel, H. El Moll, R. Utrera-Melero, M. Cordier, A. Fargues, A. Garcia, F. Massuyeau, C. Martineau-Corcos, F. Fayon, A. Rakhmatullin, S. Kahlal, J.-Y. Saillard, T. Gacoin, S. Perruchas, *Inorg. Chem.* **2018**, *57*, 4328–4339.

[44] C. Tard, S. Perruchas, S. Maron, X. F. Le Goff, F. Guillen, A. Garcia, J. Vigneron, A. Etcheberry, T. Gacoin, J.-P. Boilot, *Chem. Mater.* **2008**, *20*, 7010–7016.

[45] Q. Benito, I. Maurin, T. Cheisson, G. Nocton, A. Fargues, A. Garcia, C. Martineau, T. Gacoin, J.-P. Boilot, S. Perruchas, *Chem. Eur. J.* **2015**, *21*, 5892–5897.

[46] A. V. Shamsieva, I. E. Kolesnikov, I. D. Strelnik, T. P. Gerasimova, A. A. Kalinichev, S. A. Katsyuba, E. I. Musina, E. Lähderanta, A. A. Karasik, O. G. Sinyashin, *Phys. Chem. C* **2019**, *123*, 25863–25870.

[47] B. Huitorel, H. El Moll, M. Cordier, A. Fargues, A. Garcia, F. Massuyeau, C. Martineau-Corcos, T. Gacoin, S. Perruchas, *Inorg. Chem.* **2017**, *56*, 12379–12388.

[48] Q.-W. Guan, D. Zhang, Z.-Z. Xue, X.-Y. Wan, Z.-N. Gao, X.-F. Zhao, C.-P. Wan, J. Pan, G.-M. Wang, *Inorg. Chem. Commun.* **2018**, *95*, 144–148.

[49] S. Perruchas, C. Tard, X. F. Le Goff, A. Fargues, A. Garcia, S. Kahlal, J.-Y. Saillard, T. Gacoin, J.-P. Boilot, *Inorg. Chem.* **2011**, *50*, 10682–10692.

[50] B. Huitorel, R. Utrera-Melero, F. Massuyeau, J.-Y. Mevelec, B. Baptiste, A. Polian, T. Gacoin, C. Martineau-Corcos, S. Perruchas, *Dalton Trans.* **2019**, *48*, 7899–7909.

[51] F. De Angelis, S. Fantacci, A. Sgamellotti, E. Cariati, R. Ugo, P. C. Ford, *Inorg. Chem.* **2006**, *45*, 10576–10584.